

1 A hydrogel beads based platform for single-cell
2 phenotypic analysis and digital molecular detection

3 Yanzhe Zhu, Jing Li, Xingyu Lin, Xiao Huang, and Michael R. Hoffmann*

4 Linde+Robinson Laboratories

5 California Institute of Technology

6 Pasadena California 91125 USA

7 * Correspondence and requests for materials should be addressed to MRH

8 Tel: 626-395-4391 EM: mrh@caltech.edu

9
10
11
12
13
14
15
16
17 To be Submitted to: *Biorxiv*

18 November, 2019

Abstract

19 Microfluidic platforms integrating phenotyping and genotyping approaches have the
20 potential to advance the understanding of single cell genotype-to-phenotype correlations. These
21 correlations can play a key role in tackling antibiotic heteroresistance, cancer cell heterogeneity,
22 and other related fundamental problems. Herein, we report a novel platform that enables both high-
23 throughput digital molecular detection and single-cell phenotypic analysis, utilizing nanoliter-
24 sized biocompatible polyethylene glycol hydrogel beads produced by a convenient and disposable
25 centrifugal droplet generation device. The hydrogel beads have been demonstrated enhanced
26 thermal stability, and achieved uncompromised efficiencies in digital polymerase chain reaction,
27 digital loop-mediated isothermal amplification, and single cell phenotyping. The crosslinked
28 hydrogel network highlights the prospective linkage of various subsequent molecular analyses to
29 address the genotypic differences between cellular subpopulations exhibiting distinct phenotypes.
30 Our platform shows great potential for applications in clinical practice and medical research, and
31 promises new perspectives in mechanism elucidation of environment-evolution interaction and
32 other basic research areas.

Introduction

33 Microfluidic single cell techniques have enabled observations of rare genotypes or
34 phenotypes within a cell population and thus ubiquitous cell heterogeneity (1-3). The phenotypic
35 diversity exhibited by supposedly genetically identical cells boosts the population adaptability
36 under selection pressures, and thus raises concerns in fields spanning from clinical practice to
37 medical research on infectious diseases and cancers (4, 5), etc. For example, less susceptible
38 pathogenic bacterial subpopulations originally consist 10^{-2} to 10^{-6} of the overall population that
39 can be amplified during antibiotic exposure. The subsequent increase in the resistant subpopulation
40 may eventually lead to the failure of an antibiotic treatment (6). Hypotheses for the underlying
41 molecular mechanisms involving the stochasticity of genetic mutation, gene expression, and
42 protein regulation (7-9), however, remain hard to test in dynamically changing cell subpopulations,
43 partly due to the absence of appropriate single cell experimental technique (10). The need to better
44 understand cell heterogeneity motivates the development of new techniques that link the single-
45 cell phenotype with its *in situ* molecular information.

46 As an emerging class of technologies, water-in-oil droplet-based microfluidic platforms
47 have been well developed for high-throughput phenotypic and molecular analyses at single cell or
48 single molecule resolution (3, 11). Nonetheless, due to the rare and transient nature of cell
49 heterogeneity events, population-averaged molecular analyses would most likely fail to directly
50 explain the characterized phenotypes, even if all analyses are conducted at single cell or molecular
51 resolution (6, 12). Meanwhile, incorporating a crosslinked hydrogel network into the aqueous
52 phase theoretically provides a droplet-based platform with additional robustness by allowing
53 reagent exchange (13). This strategy, therefore, has been explored for a range of hydrogel materials
54 and crosslinking chemistry, including cooling-induced formation of agarose beads for digital

55 droplet polymerase chain reaction polymerase chain reaction (ddPCR) (14), ionic crosslinking of
56 alginate beads for cell encapsulation and DNA extraction (15, 16), UV-initiated polyethylene
57 glycol (PEG) beads for cell encapsulation (17). Such platforms have demonstrated to be effective
58 in either phenotyping or molecular analysis, while the material and/or initiation method would be
59 intrinsically incompatible with the combination of both. For example, temperature manipulation
60 or UV radiation might affect the phenotype and genotype of encapsulated cells (18), and alginate
61 is a well-known PCR inhibitor (19). PEG crosslinked by a thiol-Michael addition reaction between
62 the bioinert acrylate and thiol groups has been attempted in bulk analyses and is among the most
63 promising solutions (20, 21), but it is yet to be developed for our specific purpose. The main
64 obstacle may lie in the fast and spontaneous gelation, which would be detrimental to traditional
65 expensive microfluidic droplet generation approaches.

66 Herein, we report a novel PEG hydrogel bead-based platform, which is validated for both
67 single-cell phenotypic analysis and molecular detection (**Figure 1a-b**). To solve the challenge
68 posted by the fast thiol-Michael addition gelation chemistry, we developed a disposable centrifugal
69 device for droplet generation (**Figure 1c**). We demonstrated the effectiveness of nucleic acid
70 amplification detections, including PCR and loop-mediated isothermal amplification (LAMP),
71 through further crosslinking generated droplets into PEG hydrogel as PEG hydrogel beads
72 (Gelbeads). Compared to ddPCR and ddLAMP, Gelbead-based digital PCR and LAMP (gdPCR
73 and gdLAMP) were found to exhibit enhanced thermal stabilities and uncompromised
74 amplification efficiencies. Gelbeads were also demonstrated effective for single cell encapsulation
75 and phenotyping within 4 hr for tested bacteria. We envision that this platform will be of broad
76 interest to researchers from many fundamental fields. The Gelbead platform reported here for the
77 first time promises unprecedented capabilities for investigation of cell heterogeneity.

Results

78 **Development of the disposable droplet generation device**

79 Microfluidic-based droplet generation methods generally require special fabrication
80 facilities to fabricate sub-100 μm channels and involve complicated operation, such as syringe
81 pump-driven T-junctions fabricated by photolithography and centrifugally driven labs-on-a-disc
82 fabricated by micro milling and hot embossing (22, 23). These traditional methods are not
83 compatible with Gelbead generation due to fast clogging imposed by the thiol-Michael addition
84 chemistry. The bulk PEG crosslinking experiments showed that the time frame for droplet
85 generation before gelation was as short as 8.5 min with the chosen hydrogel concentration at 7.5
86 w/v% (**Supplementary Note 1, Table S1**). In order to easily generate Gelbeads within minutes
87 without clogging expensive microfluidic equipment, we designed a disposable device using
88 affordable commercial components (**Figure 2a**). The device utilized a dispensing blunt needle
89 with a bent tip. The bent-tipped needle was then set into a 1.5-mL microcentrifuge tube with oil to
90 establish the physics for centrifugal droplet generation. With centrifugal acceleration, the aqueous
91 phase is forced into the fluorinated oil phase by the elevated pressure difference between the
92 reservoir surface and the narrow inlet. The fluorinated oil phase with a higher density pinches off
93 the aqueous droplets, which then float to the air-oil interface.

94 Standard 20 μL LAMP mix with unquenched calcein was dispersed in fluorinated oil
95 (online methods) and characterized using a fluorescence microscope to study the droplet
96 generation performance of the device (**Figure 2b**). The average droplet size was tunable from 99
97 μm to 334 μm and the coefficient of variance (CV) was minimized to 5%, by varying the oil phase
98 volume, centrifugal acceleration, and the needle gauge as shown in **Figure 2c-f**. Smaller droplets
99 with slightly larger size distribution (**Figure 2e**) were produced by increasing the centrifugal

100 acceleration, which provided a greater pressure difference to drive the aqueous phase inflow. The
101 larger CV in **Figure 2e** was likely due to the unstable flow during initial acceleration, which can
102 be alleviated by adding more oil (**Figure 2c**) to reduce the oil phase height variation and limit the
103 amount of aqueous phase inlet during acceleration. Among all tested conditions, the optimal was
104 found to be a combination of 34 Ga needles, 80 μL oil phase, and 150 g centrifugation run for 5
105 min and droplets were produced at an average diameter of 175 μm in 5 min with minor trial-to-
106 trial difference, which was found to be comparable to other microfluidic methods such as
107 centrifugal lab-on-a-disk (22) and polymer-tube micronozzles (24) (**Supplementary Note 2**). For
108 droplets of a diameter of 175 μm , each standard 20 μL reaction could theoretically produce $\sim 10^4$
109 droplets. Based on this calculated compartmentalization, the dynamic range is theoretically from
110 0.5 to 3×10^3 target copies or cells per μL , and the detection limit is 0.1 copies or cells per μL (25).

111 **Gelbead generation and thermal stability characterization**

112 The Gelbead and droplet generation performance were assessed using various reaction
113 matrices including culture media, PCR mix, and LAMP mix, under the optimized condition
114 reported in the previous section (**Figure 3a**). The average diameter of generated Gelbeads was
115 found to range from 145 μm to 217 μm with a CV from 3.6 % to 7.6 %. The observed variations
116 were likely due to viscosity differences and interfacial property changes in different reaction
117 matrices. It should be noted that the culture media alone was not able to sustain as droplets or
118 Gelbeads in the fluorinated oil by 5% FluoroSurfactant. Bovine serum albumin (BSA), a protein
119 commonly used as an additive to protect essential molecules (fatty acids, amino acids, etc.) in
120 culture media (26), was added to the aqueous phase as an additional surfactant to modify interfacial
121 properties and thus prevent the droplet merging. For the PCR reaction matrix, the generated
122 Gelbeads had a larger CV than droplets. We assume that the presence of PEG hydrogel may have

123 disturbed the surfactant-stabilized aqueous-oil interface, by inducing interfacial adsorption of
124 additional charged species such as thiolate, magnesium ions, etc. In summary, the observed sizes
125 and CVs of droplets and Gelbeads were considered acceptable for our assays. In general, this
126 generation device fulfills the requirements for Gelbead generation. The simple generation device
127 may be used for applications for which a simple yet powerful compartmentalization method is
128 needed.

129 The effect of PEG crosslinking on stabilizing the aqueous-in-oil compartments was
130 evaluated. Thermodynamic instability of water-in oil droplets may impair the reliability of
131 amplification processes such as PCR and LAMP that require extensive heating (22). Heating
132 accelerates droplet merging and evaporation, which would affect the fluorescence reading by
133 modifying concentrations of targets and reagents (e.g., salts and fluorescent dyes). The size
134 distributions were investigated for droplets and Gelbeads before and after common heating
135 protocols respectively for PCR and LAMP (online methods, **Figure 3b**). Compared to those before
136 heating, droplets that had undergone PCR and LAMP heating increased in their CVs by 6.2% and
137 3.5%, respectively. In addition, the heating resulted in a noticeably larger population with outlier
138 sizes implying that extensive merging and evaporation had occurred. Following the same heating
139 protocol as for the droplets, the Gelbeads exhibited much less of a change in size distribution (CV
140 increased by 1.9% for PCR and 1.6% for LAMP), however the average Gelbead diameter
141 decreased slightly. These results indicate that the stabilization effect achieved by crosslinked PEG
142 was mainly by prevention of the merging of beads. Gelbeads used for the LAMP procedure had a
143 more significant improvement in thermal stability due to PEG crosslinking than for the PCR
144 procedure. We assume that, in the case of the PCR recipe, the combination of SuperMix and the
145 oil phase from BioRad were chemically well-optimized for interfacial stability, leaving limited

146 room for improvement. This result therefore indicates that, other than modifying the surfactant
147 composition or increasing surfactant concentration, hydrogel crosslinking could be an alternative
148 strategy for maintaining the emulsion. Our results demonstrate that Gelbeads are a reliable
149 platform for standalone heated digital analysis in terms of enhanced individual compartment
150 integrity.

151 **Gelbead digital PCR (gdPCR)**

152 To validate the reliability of gdPCR, we compared gdPCR to digital PCR performed in
153 droplets generated from a commercial recipe (represented as ddPCR, hereinafter) for amplification
154 efficiency with DNA extracted from cultured *Salmonella* Typhi (*S. Typhi*). Previous use of
155 hydrogels and PCR utilized polyacrylamide in the form of either a bulk phase hydrogel membrane
156 as a quasi-digital PCR platform (27) or using hydrogel beads as a substrate for surface coating of
157 primers (28, 29), which is an approach opposite to our concept. To the best of our knowledge,
158 performing PCR inside crosslinked hydrogel beads has not been reported to date. Even in bulk
159 membrane form, only 80% amplification efficiency was observed, which may be partially
160 attributed to template damage by free radicals as suggested (27). In this study, a similar drop in
161 amplification efficiency was observed in the Gelbeads compared to that in droplets (**Figure 4a**),
162 even though the Michael addition chemistry between acrylate and thiol used in this study does not
163 involve free radical formation. In this case, crosslinked hydrogel network may be responsible for
164 the observed inhibition by limiting the diffusion of functional components such as ions, nucleic
165 acids, and proteins, where the extent of the limitation relates to the size and charge of the
166 component (30, 31). From effective diffusivity modeling (**Figure S1**), we reasoned that the most
167 affected functional component might be DNA polymerase, which is the relatively large protein
168 (~6 nm) responsible for building amplicons. For a fixed template concentration of 200 copies/ μ L

169 estimated by ddPCR, gdPCR assay performance was assessed with additional OneTaq polymerase
170 supplied at varying concentrations of 0.025, 0.05, 0.1, 0.2 Units per reaction, as shown in **Figure**
171 **4a**. Results showed that additional 0.025 Unit per reaction, 5% of the recommended OneTaq
172 polymerase concentration per reaction, boosted the amplification efficiency the most. OneTaq
173 polymerase concentrations supplied more or less than that showed inhibition to amplification
174 efficiency, and gdPCR assay with additional 0.2 Unit per reaction was shown to be completely
175 inhibited. We speculate that the observed trend was mainly due to the commercial SuperMix buffer
176 conditions not optimized for the supplied OneTaq polymerase. While some additional polymerase
177 compensated the reduced diffusivity of the SuperMix polymerase in hydrogel, the excess
178 additional OneTaq polymerase might scavenge the essential ions for the original polymerase from
179 SuperMix leading to amplification failure. With the optimized additional polymerase, gdPCR
180 assays for serially diluted DNA with concentrations ranging from 2.5 to 600 copies/ μ L were then
181 performed; typical images are shown in **Figure 4c-h (Supplementary Note 3)**. The image analysis
182 results demonstrated that the amplification efficiency of gdPCR was comparable ($k = 0.98 \pm 0.02$,
183 $R^2 = 0.9979$) to that of ddPCR with the recipe adjustment (**Figure 4b**). The quantification results
184 also correlated well with input DNA concentration (**Figure S2a**). It should be noted that the
185 crosslinking inhibition effect eliminated in this case was for a 131 bp target gene (32), a typical
186 size for detection of specific bacteria. Further optimization in polymerase or Supermix
187 concentration would be required for other applications if a larger DNA fragment is targeted.

188 **Gelbeads digital LAMP (gdLAMP)**

189 Gelbeads applied in digital LAMP were also investigated. LAMP has been an attractive
190 emerging platform for molecular detection since it eliminates the need for thermocycling by
191 utilizing a combination of 4 or 6 primers to achieve fast and specific detection (33). The heating

192 protocol of LAMP was fairly mild, however, severe Gelbead aggregation occurred for samples
193 with target DNA but not for no-template controls (**Figure S3**) in preliminary experiments. This
194 was supposedly due to the fact that LAMP produces a much larger amount of amplification
195 products than PCR (33). The negatively charged amplified DNA may have affected interfacial
196 tension when adsorbed to the interface. Aggregated Gelbeads showed apparent crosstalk, which
197 rendered the assay invalid since the compartment independence assumption required for Poisson
198 statistics was contradicted. The problem was relieved by adding 1.5 mg/mL BSA, a common real-
199 time PCR additive, to prevent surface adsorption. However, it was still observed that positive
200 Gelbeads tended to stick next to each other (**Figure 5a**). The observed radiative patterns in
201 Gelbeads manifested the differential diffusivity of amplification products of varying size in
202 crosslinked hydrogel network. A similar radiative pattern was observed by Huang et al. in LAMP
203 performed in a hydrogel membrane (21). In our case, neither of the two radiative centers were at
204 the connected interface, indicating that the stickiness may not have led to false positive Gelbeads
205 within the time frame tested. The connection of positive Gelbeads was most likely the result of a
206 change in interfacial tension caused by large amount of the negatively charged DNA produced
207 during amplification. Further crosslinking breaking through the oil barrier would only occur when
208 the positive Gelbeads encounter each other. In summary, the connected interface should not affect
209 the quantification results. The gdLAMP quantifications for no-template control and serial diluted
210 *S. Typhi* DNA ranging from 300 to 1.2×10^4 copies/ μ L were then verified. Example images are
211 shown in **Figure 5c-h**. The image analysis results demonstrated that the amplification efficiency
212 of gdLAMP was similar ($k = 1.01 \pm 0.01$, $R^2 = 0.9996$) to that of ddLAMP (**Figure 5b**). However,
213 both ddLAMP and gdLAMP gave concentration estimations ~2 orders of magnitude lower than
214 input DNA concentration (**Figure S2b**). Further increases in the amplification efficiency would

215 likely require an improved primer design, which is out of the scope of this study. In summary, the
216 results confirmed our hypothesis that the stickiness of positive Gelbeads do not considerably affect
217 gdLAMP quantification, and demonstrated that the hydrogel network had a negligible inhibition
218 effect on the digital LAMP assays that were performed.

219 **Gelbeads for cell phenotyping**

220 For single cell phenotyping, we first validated single cell encapsulation efficiency using
221 *Salmonella* Typhimurium with green fluorescent protein (GFP). The cells were diluted to an
222 average of 1 cell per Gelbead for counting the number of cells in each Gelbead (**Figure 6b**). At
223 this cell concentration, theoretically, 34% of the compartments were occupied by single cells,
224 which was the maximum following a Poisson distribution, 29% of the compartments encapsulated
225 more than 1 cell, and 37% of the compartments contained no cells. As shown in **Figure 6a**, the
226 observed number of encapsulated cells was close to the theoretical distribution. Gelbeads with high
227 cell numbers were slightly less than predicted, possibly because some cells were located out of
228 focus when imaged in spherical compartments at a high microscope objective. Since high
229 throughput detection of stained cells within spherical compartments droplets or Gelbeads was
230 challenging for fluorescence microscope imaging, we chose to employ cell metabolism indicator
231 dye in Gelbead phenotyping experiments. As a resazurin-based dye used in bulk phenotyping
232 assays of a wide range of cell lines, alamarBlue can be reduced by actively metabolizing cells into
233 resorufin, whose bright red fluorescence can stain the whole compartment for visualization (34).
234 Phenotyping of *S. Typhi* in Gelbeads was investigated by co-incubation of alamarBlue and *S.*
235 *Typhi* in the culture media. The fluorescence of Gelbeads was monitored during the incubation for
236 up to 4 hrs (**Figure 6d-h**). It was observed that Gelbeads appeared to be much brighter than the
237 droplets were before incubation (**Figure S4**); this was possibly due to additional reduction of

238 resazurin by thiol group (35). We suppose that the interference by thiol groups would not affect
239 the phenotyping results since the monomers were rigorously mixed and evenly distributed into
240 Gelbeads. Gelbeads containing live cells would exhibit even brighter fluorescence in the presence
241 of sufficient AlamarBlue. The quantitative performance of Gelbead phenotyping was verified by
242 analysis of observed fractions of bright fluorescent Gelbeads (see online methods and **Figure S5**
243 for thresholding) compared to the theoretical value, as shown in **Figure 6c**. 63% of Gelbeads were
244 supposed to contain greater than or equal to 1 cell and thus to be bright. The observed positive
245 fraction of $62.0 \pm 1.5\%$ after 4 hours of incubation matched well with the theoretical value of 63%.
246 It was also noticed that, after 3 hours of incubation, the positive Gelbead fraction was $36.4 \pm 8.1\%$,
247 which corresponds well with the theoretical fraction of Gelbeads (29%) encapsulating more than
248 1 cell. Based on the linear response of alamarBlue to the number of cells within the compartment
249 (36), our results reasonably indicate that effective single cell phenotyping in Gelbeads is
250 achievable within 4 hrs. However, 5 hr incubation lead to overly bright fluorescence and $92.9 \pm 2.7\%$
251 bright Gelbeads, which was likely attributed to excessive incubation and the diffusion of
252 metabolized fluorescent resorufin across the aqueous-oil interfacial barrier. Our results indicate
253 that the optimization of incubation time is a race between cross-talking and cell proliferation.
254 Considering the intrinsic difference in proliferation rate between bacterial species, the observed
255 incubation time for distinction of positive and negative compartments was comparable to the
256 results by Lyu et al., who achieved *Escherichia coli* (*E. coli*) phenotyping with alamarBlue in 85
257 pL droplets with a 2 hr incubation (3). We note that, although the single cell encapsulated Gelbeads
258 were maximized and theoretically comprised the majority (54%) of the bright Gelbeads in the
259 current set up, strategies are available to break Poisson distribution for higher single cell
260 encapsulation rates, such as microvortex-aided hydrodynamic trapping and then releasing single

261 cells to droplets (37). In summary, the cell viability detection strategy demonstrated with Gelbeads
262 has been proved to apply well to a wide range of cells in bulk assays and droplet microfluidics (3,
263 34, 36). Thus, the Gelbeads synthesized in this study provide a suitable platform for phenotyping
264 cell heterogeneity, if they are co-encapsulated with antibiotics or drugs.

Discussion

265 The developed Gelbeads platform promises a robust analysis tool that has the potential to
266 link single-cell phenotypic analysis with reliable *in situ* molecular detection together. Besides the
267 advantages presented, we acknowledge the following limitations. First, the dynamic range in our
268 study was restricted by the size of the compartments generated by our device. Further reductions
269 in size would result in larger size variations, and the surfactant might have to be changed or
270 adjusted if higher uniformity is required. Second, given the use of fluorescence microscopic
271 imaging of the compartments inside a viewing chamber, the Gelbead imaging approach employed
272 could probe only a limited viewing area, and the resolution could be affected by the focus. The
273 fluorescence characterization may be further improved by flow cytometry to interrogate single
274 Gelbeads.

275 In this work, a disposable centrifugal device was developed for Gelbead generation using
276 highly biocompatible PEG monomers spontaneously crosslinked with no free-radical, UV-induced
277 or heat-induced initiation. Our design allows for easy use of droplet microfluidics without
278 expensive and complicated equipment, which could be useful for applications other than Gelbeads
279 generation. In addition to the single cell phenotyping potential, the Gelbeads approach has
280 enhanced thermal stability coupled with high amplification efficiency for dPCR and dLAMP.
281 Widely available qPCR and LAMP assays can therefore be easily transferred into digital assays
282 by this Gelbeads approach. The unique structural stability of the hydrogel network allows for easy

283 manipulation of the Gelbeads that may have many possibilities for other upstream and downstream
284 analyses. The Gelbead platform will be further developed for reagent exchange, fluorescence-
285 based Gelbead sorting, and downstream sequencing, etc. We envision that the potential of our
286 Gelbeads platform in generating genetic and gene expression data with phenotyped single cells
287 will help narrow the genotype-phenotype gap and thus offer exciting new insights in cell
288 heterogeneity studies.

Materials and Methods

289 **PEG crosslinking and characterizations**

290 PEG hydrogel monomers included 4-arm PEG-acrylate [molecular weight (MW) of 10 000,
291 Laysan Bio, Arab, AL, USA] and thiol-PEG-thiol (MW of 3400; Laysan Bio), with acrylate and
292 thiol mixed at a molar ratio of 1:1 for crosslinking. For sol-gel transition time characterization, 7.5
293 w/v% and 10 w/v% PEG hydrogel were respectively tested in PCR mix, LAMP mix, and culture
294 media mix. PEG monomers were weighed to make 10× monomer solutions for PEG-acrylate and
295 PEG-thiol separately. The weighed monomers were then dissolved either in water (Molecular
296 Biology Grade Water, Corning, Acton, MA, USA) for PCR and LAMP mix, or in TSB (BD™
297 Bacto™ Tryptic Soy Broth, Becton Dickinson and Company, Franklin Lakes, NJ, USA) for culture
298 media mix. In addition to 2 μL of each 10× PEG monomer solution, for each 20 μL reaction mix,
299 PCR mix contained 10 μL ddPCR Supermix for Probes (BioRad, Hercules, CA, USA) and 6 μL
300 water; LAMP mix contained 10 μL 2×WarmStart LAMP Mastermix (New England Biolabs,
301 Ipswich, MA, USA) and 6 μL water; culture media mix contained 16 μL TSB. The reaction mix
302 was briefly vortexed. The sol-gel transition was considered started when lifting the pipette tip
303 could draw filaments out of the reaction mix, and the transition was considered ended when the
304 reaction mix formed a gelatinous lump.

305 **Development of the disposable droplet generation device**

306 Each droplet generation device consisted of a 1.5 mL DNA LoBind tube (Eppendorf,
307 Hamburg, Germany) and a blunt tip dispensing needle (LAOMA Amazon, Seattle, WA, USA)
308 with the tip bent by a tweezer (VWR, Radnor, PA, USA). The tweezer and the needles were
309 autoclaved (2540EP, Heidolph Brinkmann, Schwabach, Germany) prior to use. The oil phase was
310 added to the bottom of the microcentrifuge tube, and the aqueous reaction mix was added to the

311 Luer-lock of the needle. The device was then centrifuged (Centrifuge 5430R, Eppendorf) for 5
312 min. For optimization of droplet generation, fluorinated oil (HFE-7500 3M[®] Novec[®] Engineering
313 Fluid, 3M, Maplewood, MN, USA) supplied with 5% FluoroSurfactant (RAN Biotechnologies,
314 Beverly, MA, USA) was added into the oil phase. The 20- μ L aqueous phase contained
315 1 \times WarmStart LAMP Mastermix and 50 μ M calcein (Sigma-Aldrich, St. Louis, MO, USA). Four
316 parameters including oil phase volume, needle inner diameter, centrifugal acceleration and oil
317 volume added to the Luer-lock were investigated. Specific variables in details were as follows: 1)
318 the oil phase volume of 40, 60, 80 and 100 μ L, respectively, at the bottom of the tube in 34 Ga
319 needles under 250 g centrifugation; 2) needles of 30, 32 and 34 Ga (corresponding to inner
320 diameter of around 160, 110 and 80 μ m) under the condition of 250 g centrifugation and 80 μ L oil
321 phase volume; 3) the centrifugal accelerations of 50, 150, 250, 500, 1000 g with 34 Ga needles
322 and 80 μ L oil phase; 4) additional oil phase added into the Luer-lock of 0, 10 and 20 μ L in 34 Ga
323 needles under 250 g centrifugation with 80 μ L oil phase.

324 **Gelbead generation and thermal stability characterization**

325 In all the following experiments, the device configuration was fixed with 34 Ga needles,
326 80 μ L oil phase, no additional oil at the Luer-lock, and 150 g centrifugation run for 5 min. The
327 droplet and Gelbead generation using the described device was respectively characterized with
328 PCR mix, LAMP mix, and culture media mix. In each 20 μ L reaction, the PCR mix contained 1 \times
329 ddPCR Supermix and 50 μ M calcein; the LAMP mix contained 1 \times WarmStart LAMP Mastermix,
330 and 50 μ M calcein; the culture media mix was TSB with 1 mg/mL BSA (New England Biolabs)
331 and 50 μ M calcein. The mix was briefly pipette mixed. The reaction mix for Gelbead generation
332 contained 7.5 w/v% PEG hydrogel, added as 10 \times PEG monomers. For dispersion of PCR mix as

333 droplets and Gelbeads, Droplet Generation Oil for Probes (BioRad) was used instead of fluorinated
334 oil with 5% FluoroSurfactant.

335 For thermal stability characterizations, generated droplets or Gelbeads were extracted into
336 PCR tubes (0.2 mL individual PCR tubes, BioRad) and incubated in a thermal cycler (T100,
337 BioRad). The thermocycling protocol for PCR included 10 min of initiation at 95 °C, followed by
338 40 cycles of denaturation at 94 °C for 30 s, annealing at 52 °C for 60 s, and extension at 65 °C for
339 30 s. For LAMP heating, droplets or Gelbeads were incubated at 65 °C for 1 hour.

340 **Bacterial Cell culture and DNA preparation**

341 *Salmonella* Typhi (*S. Typhi*, CVD 909), obtained from American Type Culture Collection
342 (ATCC, Manassas, VA, USA), was employed as the model strain. *S. Typhi* was cultivated in TSB
343 supplied with 1 mg/L of 2,3-dihydroxybenzoate (DHB, Sigma-Aldrich) in an incubator (Innova
344 42, New Brunswick Scientific, Edison, NJ, USA) shaking at 200 rpm at 35 °C for 14-16 hours.
345 The concentration of cultivated cells was estimated by OD 600 (NanoDrop 2000c
346 Spectrophotometer, Thermo Scientific, Barrington, IL, USA). DNA was harvested using
347 PureLink® Genomic DNA Mini Kits (Fisher Scientific, Waltham, MA, USA) following the
348 manufacturer's instructions. For single cell encapsulation test, *Salmonella* Typhimurium GFP
349 (ATCC 14028GFP) was cultivated in nutrient broth (Difco™ 23400, Becton Dickinson and
350 Company) supplied with 100 mcg/ml Ampicillin (Sigma-Aldrich) in an incubator shaking at 200
351 rpm at 37 °C for 14-16 hours. The cell concentration was estimated by counting under a
352 fluorescence microscope (Leica DMI8, Wetzlar, Germany).

353 **Gelbead Digital PCR (gdPCR) assay**

354 The thermocycling protocol of gdPCR assay was the same as described in the thermal
355 stability characterization. Each 20 µL reaction consisted of 1× ddPCR Supermix, 900 nM forward

356 primer, 900 nM reverse primer, 250 nM probe, and 2 μ L DNA sample or water. Additional 7.5
357 w/v% PEG hydrogel was added as 10 \times PEG monomers for gdPCR assays. The primers and probe
358 were ordered from Integrated DNA Technologies (IDT, Coralville, IA, USA), with sequences
359 (**Supplementary Table S1**) designed for specific detection of *S. Typhi*, targeting a region in gene
360 STY0201 for an amplicon size of 131 bp (32). For gdPCR optimization, the same DNA template
361 concentration (600 times dilution from harvested) was added for gdPCR assays and ddPCR control.
362 Optimal concentration of additional polymerase (OneTaq[®] DNA polymerase, New England
363 Biolabs) was investigated by supplying various concentrations to the described reaction mix
364 incrementally at 0.025, 0.5, 0.1 and 0.2 U/reaction. For quantification assays, harvested DNA
365 sample were serial diluted 100, 300, 600, 1500, and 24000 times for ddPCR and gdPCR. The
366 reactions were prepared on iceblock (Carolina[®] Chill Block, Burlington, NC, USA) and
367 centrifugation temperature was set at 4 $^{\circ}$ C. Droplets or Gelbeads were generated in BioRad droplet
368 generation oil, and were then extracted into PCR tubes for thermocycling. No-template controls
369 were examined for each tested condition.

370 **Gelbead Digital LAMP (gdLAMP) assay**

371 The reagents for LAMP were acquired from New England BioLabs if not indicated
372 otherwise. Each 20 μ L of modified LAMP mix for digital single bacteria LAMP contained 1 \times
373 isothermal buffer, 6 mM total MgSO₄, 1.4 mM dNTP, 640 U/mL Bst 2.0 WarmStart polymerase,
374 1.6 μ M FIB and BIP, 0.2 μ M F3 and B3, 0.8 μ M LF and LB, 1.5 mg/mL BSA, 1 \times LAMP dye (38).
375 For gdLAMP assays, 7.5 w/v% PEG hydrogel was added as 10 \times PEG monomers. The primers,
376 ordered from IDT with the sequences shown in **Supplementary Table S1**, were targeting a 196
377 bp region within the *S. Typhi* specific gene STY1607 (39). For gdLAMP and ddLAMP assays,
378 harvested DNA was serial diluted 5, 20, 50, 100, and 200 times. The reactions were prepared on

379 iceblock and centrifuged into 5% FluoroSurfactant supplied fluorinated oil at 4 °C. Droplets or
380 Gelbeads were then extracted into PCR tubes for 30 min heating at 65 °C followed by 5 min
381 polymerase deactivation at 80 °C. No-template controls were examined under the same protocol.

382 **Single cell phenotyping**

383 For single cell encapsulation efficiency test, the cultivated *Salmonella* Typhimurium GFP
384 was diluted 600 times for Gelbeads generation. The dilution factor was estimated from prior
385 knowledge of cultured cell concentration and Gelbead volume. The number of cells encapsulated
386 in each Gelbead was analyzed by fluorescence microscope imaging with a 20× objective. 79
387 Gelbeads were analyzed from 15 fluorescent images. For phenotyping experiments, 1mL of
388 overnight cultured *S. Typhi* was freshly cultivated for 3 hours in 5mL TSB supplied with 1 mg/L
389 of DHB in an incubator shaking at 200 rpm at 35 °C. The cell concentration was verified to be
390 around 0.135 by OD 600. AlamarBlue (Invitrogen, Carlsbad, CA, USA) was employed as the cell
391 viability indicator. To address the fluctuation of excitation intensity and emission detection within
392 a microscopic view, calcein was used as a reference dye. Each 20 µL reaction consisted of 1×
393 AlamarBlue, 50 µM calcein, 1 mg/mL BSA, diluted *S. Typhi* cells, and the rest of the volume filled
394 with DHB supplied TSB. 7.5 w/v% PEG hydrogel was added as 10× PEG monomers dissolved in
395 DHB supplied TSB. After generation, the Gelbeads were incubated at 37 °C for 0-5 hrs. Gelbeads
396 were extracted for imaging after 0, 1, 2, 3, 4 hrs of incubation.

397 **Droplets and Gelbeads imaging and analysis**

398 The droplets or Gelbeads to be analyzed were pipetted into a viewing chamber made by
399 adhering SecureSeal™ Hybridization Chamber (9 mm DIA × 1.0 mm Depth, Grace Bio-Labs,
400 Bend, OR, USA) to a glass slide (VistaVision® Microscope slides, VWR). The chambers were
401 imaged under the fluorescence microscope using a 1.25× objective for droplets/Gelbeads

402 generation, characterizations, and gdLAMP. For each sample in gdPCR and single cell
403 phenotyping, five images of different area in the viewing chamber were taken using a 5× objective.
404 Fluorescein isothiocyanate (FITC) filter was used, except for phenotyping experiments where
405 Texas Red (TXR) filter was used in addition. In phenotyping experiments, the image data collected
406 through TXR channel was normalized using the image data collected through FITC channel. For
407 analysis of bright Gelbeads fraction, the data of each pixel was the intensity ratio of TXR channel
408 to FITC channel. All images were analyzed using customized MATLAB scripts (**Supplementary**
409 **Files**). For droplets and Gelbeads generation as well as thermal stability characterizations, the
410 images were analyzed for individual compartment diameters. The diameters were further analyzed
411 to calculate average compartment diameter and coefficient of variation (CV). For gdPCR,
412 gdLAMP, and phenotyping assays, in addition to size analysis, the images were also analyzed for
413 number of positive and negative compartments by setting a bright-dark threshold. Using the ratio
414 of negative compartments to total compartments, the input DNA or cell concentrations were
415 estimated by Poisson distribution (40). For images from phenotyping assays, since the distinction
416 of dark and bright Gelbeads was hard to inspect visually, Gaussian fitting was used to advice the
417 threshold (**Figure S5**).

Reference

- 418 1. C. M. O'Keefe *et al.*, Facile profiling of molecular heterogeneity by microfluidic digital melt. *Sci*
419 *Adv* **4**, (2018).
- 420 2. L. F. Cheow *et al.*, Single-cell multimodal profiling reveals cellular epigenetic heterogeneity. *Nat*
421 *Methods* **13**, 833-836 (2016).
- 422 3. F. J. Lyu *et al.*, Phenotyping antibiotic resistance with single-cell resolution for the detection of
423 heteroresistance. *Sensor Actuat B-Chem* **270**, 396-404 (2018).
- 424 4. I. El Meouche, M. J. Dunlop, Heterogeneity in efflux pump expression predisposes antibiotic-
425 resistant cells to mutation. *Science* **362**, 686+ (2018).
- 426 5. D. Shibata, Cancer. Heterogeneity and tumor history. *Science* **336**, 304-305 (2012).
- 427 6. D. I. Andersson, H. Nicoloff, K. Hjort, Mechanisms and clinical relevance of bacterial
428 heteroresistance. *Nat Rev Microbiol*, (2019).
- 429 7. U. Ben-David *et al.*, Genetic and transcriptional evolution alters cancer cell line drug response.
430 *Nature* **560**, 325-330 (2018).
- 431 8. A. Harms, E. Maisonneuve, K. Gerdes, Mechanisms of bacterial persistence during stress and
432 antibiotic exposure. *Science* **354**, (2016).
- 433 9. H. Nicoloff, K. Hjort, B. R. Levin, D. I. Andersson, The high prevalence of antibiotic
434 heteroresistance in pathogenic bacteria is mainly caused by gene amplification. *Nat Microbiol* **4**,
435 504-514 (2019).
- 436 10. V. Takhaveev, M. Heinemann, Metabolic heterogeneity in clonal microbial populations. *Curr Opin*
437 *Microbiol* **45**, 30-38 (2018).
- 438 11. E. A. Ottesen, J. W. Hong, S. R. Quake, J. R. Leadbetter, Microfluidic digital PCR enables
439 multigene analysis of individual environmental bacteria. *Science* **314**, 1464-1467 (2006).
- 440 12. A. Marusyk, V. Almendro, K. Polyak, Intra-tumour heterogeneity: a looking glass for cancer? *Nat*
441 *Rev Cancer* **12**, 323-334 (2012).

- 442 13. Y. S. Zhang, A. Khademhosseini, Advances in engineering hydrogels. *Science* **356**, (2017).
- 443 14. Z. Zhu *et al.*, Highly sensitive and quantitative detection of rare pathogens through agarose droplet
444 microfluidic emulsion PCR at the single-cell level. *Lab on a Chip* **12**, 3907-3913 (2012).
- 445 15. W. H. Tan, S. Takeuchi, Monodisperse alginate hydrogel microbeads for cell encapsulation.
446 *Advanced Materials* **19**, 2696-+ (2007).
- 447 16. P. Zimny, D. Juncker, W. Reisner, Hydrogel droplet single-cell processing: DNA purification,
448 handling, release, and on-chip linearization. *Biomicrofluidics* **12**, (2018).
- 449 17. C. J. Young, L. A. Poole-Warren, P. J. Martens, Combining submerged electrospray and UV
450 photopolymerization for production of synthetic hydrogel microspheres for cell encapsulation.
451 *Biotechnol Bioeng* **109**, 1561-1570 (2012).
- 452 18. H. Ikehata, T. Ono, The Mechanisms of UV Mutagenesis. *J Radiat Res* **52**, 115-125 (2011).
- 453 19. R. M. Wadowsky, S. Laus, T. Libert, S. J. States, G. D. Ehrlich, Inhibition of Pcr-Based Assay for
454 Bordetella-Pertussis by Using Calcium Alginate Fiber and Aluminum Shaft Components of a
455 Nasopharyngeal Swab. *Journal of Clinical Microbiology* **32**, 1054-1057 (1994).
- 456 20. L. Xu, I. L. Brito, E. J. Alm, P. C. Blainey, Virtual microfluidics for digital quantification and
457 single-cell sequencing. *Nat Methods* **13**, 759-762 (2016).
- 458 21. X. Huang *et al.*, Smartphone-Based in-Gel Loop-Mediated Isothermal Amplification (gLAMP)
459 System Enables Rapid Coliphage MS2 Quantification in Environmental Waters. *Environ Sci*
460 *Technol* **52**, 6399-6407 (2018).
- 461 22. F. Schuler *et al.*, Centrifugal step emulsification applied for absolute quantification of nucleic acids
462 by digital droplet RPA. *Lab on a Chip* **15**, 2759-2766 (2015).
- 463 23. Y. C. Tan, V. Cristini, A. P. Lee, Monodispersed microfluidic droplet generation by shear focusing
464 microfluidic device. *Sensor Actuat B-Chem* **114**, 350-356 (2006).
- 465 24. S. Haeberle *et al.*, Alginate bead fabrication and encapsulation of living cells under centrifugally
466 induced artificial gravity conditions. *J Microencapsul* **25**, 267-274 (2008).

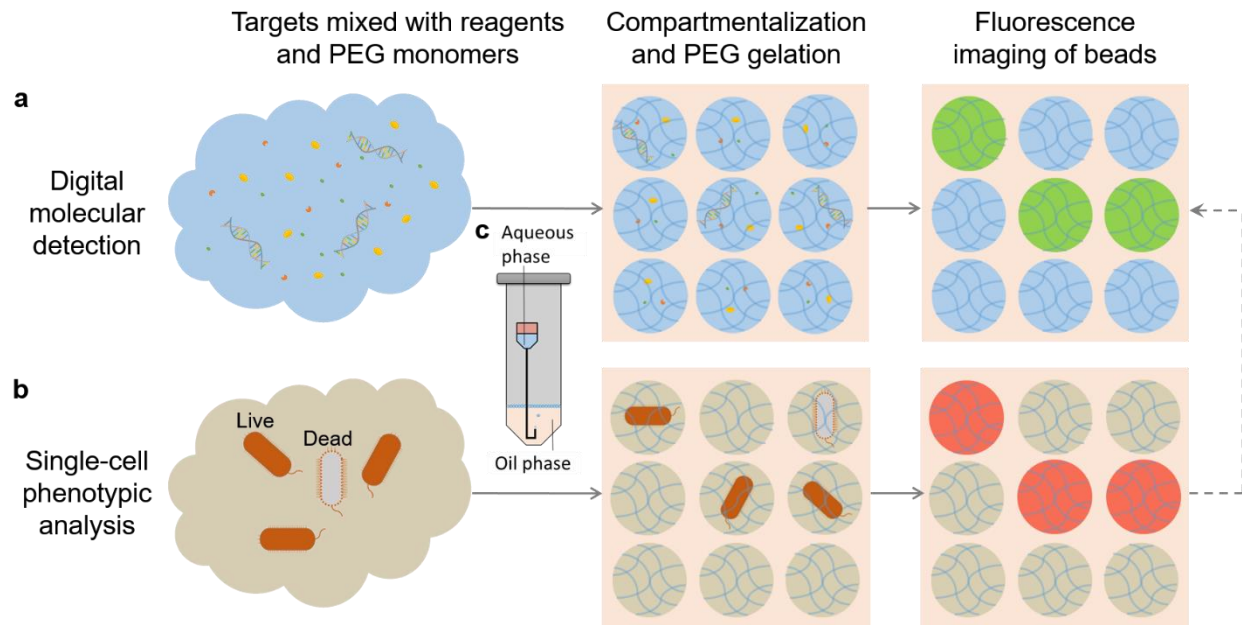
- 467 25. J. E. Kreutz *et al.*, Theoretical design and analysis of multivolume digital assays with wide dynamic
468 range validated experimentally with microfluidic digital PCR. *Anal Chem* **83**, 8158-8168 (2011).
- 469 26. G. L. Francis, Albumin and mammalian cell culture: implications for biotechnology applications.
470 *Cytotechnology* **62**, 1-16 (2010).
- 471 27. R. D. Mitra, G. M. Church, In situ localized amplification and contact replication of many
472 individual DNA molecules. *Nucleic Acids Res* **27**, (1999).
- 473 28. S. J. Spencer *et al.*, Massively parallel sequencing of single cells by epicPCR links functional genes
474 with phylogenetic markers. *Isme J* **10**, 427-436 (2016).
- 475 29. R. Zilionis *et al.*, Single-cell barcoding and sequencing using droplet microfluidics. *Nature*
476 *Protocols* **12**, (2017).
- 477 30. L. M. Weber, C. G. Lopez, K. S. Anseth, Effects of PEG hydrogel crosslinking density on protein
478 diffusion and encapsulated islet survival and function. *J Biomed Mater Res A* **90a**, 720-729 (2009).
- 479 31. Y. B. Wu, S. Joseph, N. R. Aluru, Effect of Cross-Linking on the Diffusion of Water, Ions, and
480 Small Molecules in Hydrogels. *J Phys Chem B* **113**, 3512-3520 (2009).
- 481 32. V. T. N. Tran *et al.*, The sensitivity of real-time PCR amplification targeting invasive Salmonella
482 serovars in biological specimens. *Bmc Infectious Diseases* **10**, (2010).
- 483 33. T. Notomi *et al.*, Loop-mediated isothermal amplification of DNA. *Nucleic Acids Res* **28**, E63
484 (2000).
- 485 34. M. L. Xu, D. J. McCanna, J. G. Sivak, Use of the viability reagent PrestoBlue in comparison with
486 alamarBlue and MTT to assess the viability of human corneal epithelial cells. *J Pharmacol Tox*
487 *Met* **71**, 1-7 (2015).
- 488 35. B. H. Neufeld, J. B. Tapia, A. Lutzke, M. M. Reynolds, Small Molecule Interferences in Resazurin
489 and MTT-Based Metabolic Assays in the Absence of Cells. *Anal Chem* **90**, 6867-6876 (2018).
- 490 36. J. Shemesh *et al.*, Stationary nanoliter droplet array with a substrate of choice for single
491 adherent/nonadherent cell incubation and analysis. *Proc Natl Acad Sci U S A* **111**, 11293-11298
492 (2014).

- 493 37. E. Um, S. G. Lee, J. K. Park, Random breakup of microdroplets for single-cell encapsulation. *Appl*
494 *Phys Lett* **97**, (2010).
- 495 38. X. Lin, X. Huang, K. Urmann, X. Xie, M. R. Hoffmann, Digital Loop-Mediated Isothermal
496 Amplification on a Commercial Membrane. *ACS Sens* **4**, 242-249 (2019).
- 497 39. F. X. Fan, M. Y. Yan, P. C. Du, C. Chen, B. Kan, Rapid and Sensitive Salmonella Typhi Detection
498 in Blood and Fecal Samples Using Reverse Transcription Loop-Mediated Isothermal Amplification.
499 *Foodborne Pathogens and Disease* **12**, 778-786 (2015).
- 500 40. L. B. Pinheiro *et al.*, Evaluation of a Droplet Digital Polymerase Chain Reaction Format for DNA
501 Copy Number Quantification. *Analytical Chemistry* **84**, 1003-1011 (2012).
- 502

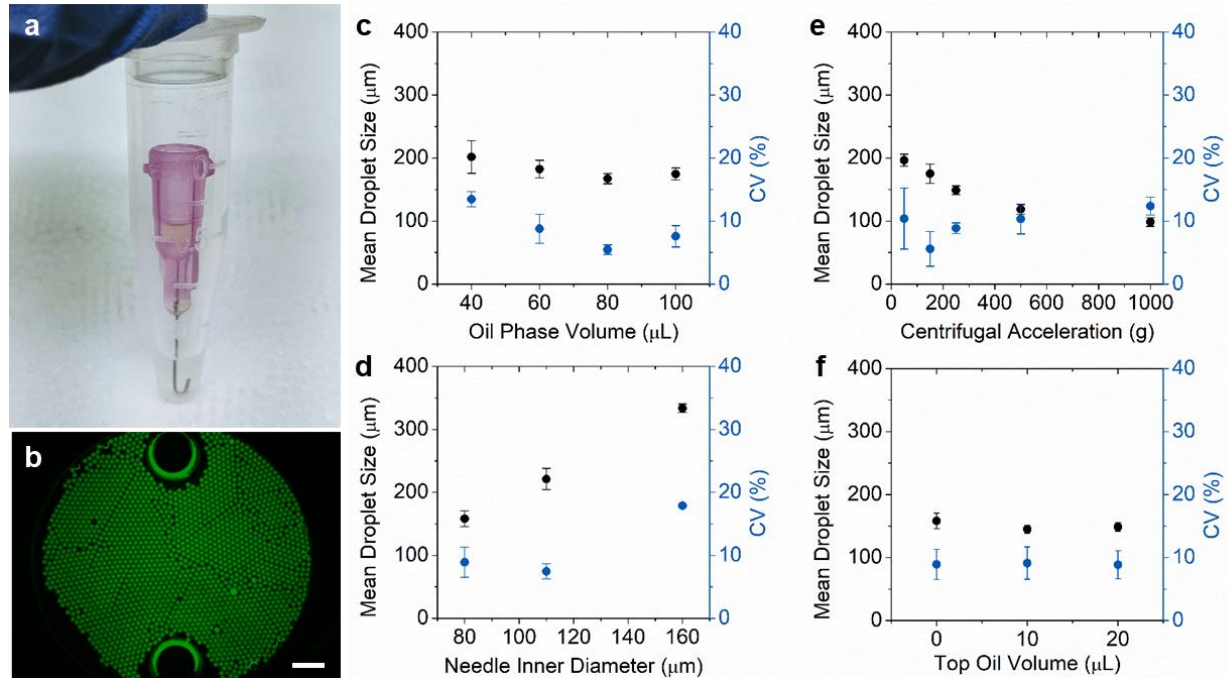
503 **Acknowledgment:**

504 **General:** We thank Dr. Katharina Urmann for helpful discussions. **Funding:** The authors
505 acknowledge the financial support provided by the Bill and Melinda Gates Foundation (grant nos.
506 OPP1111252 and OPP1192379). **Author contributions:** The manuscript was written through
507 contributions of all authors. M.R.H, X.H., and Y.Z. conceived the concept for this study. J.L.,
508 X.H., X.L. and Y.Z. designed the study, Y.Z. performed experiments, and J.L. and Y.Z. wrote the
509 paper. All authors approved of the manuscript. **Competing interests:** The authors declare no
510 competing financial interests. **Data and materials availability:** The manuscript and the
511 supplementary materials contain all data needed to evaluate the conclusions in the paper.
512 Correspondence and requests for materials should be addressed to M.R.H.

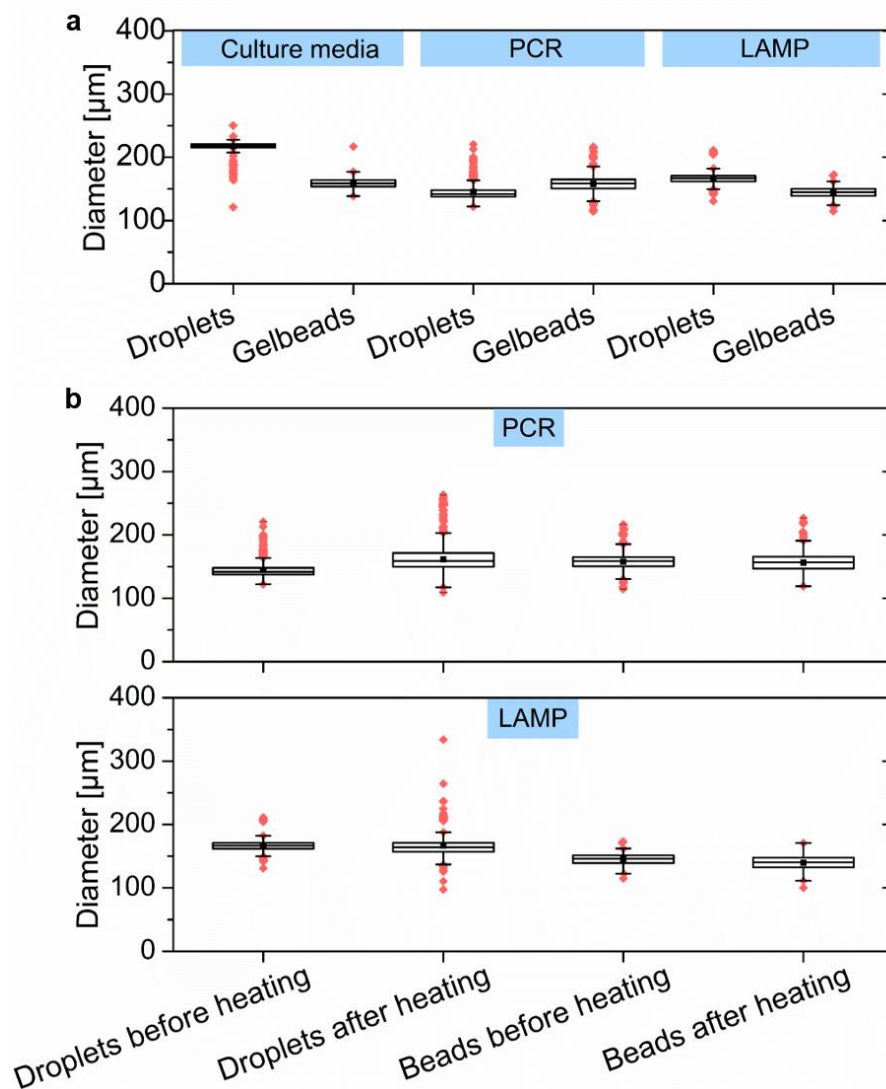
Display Items



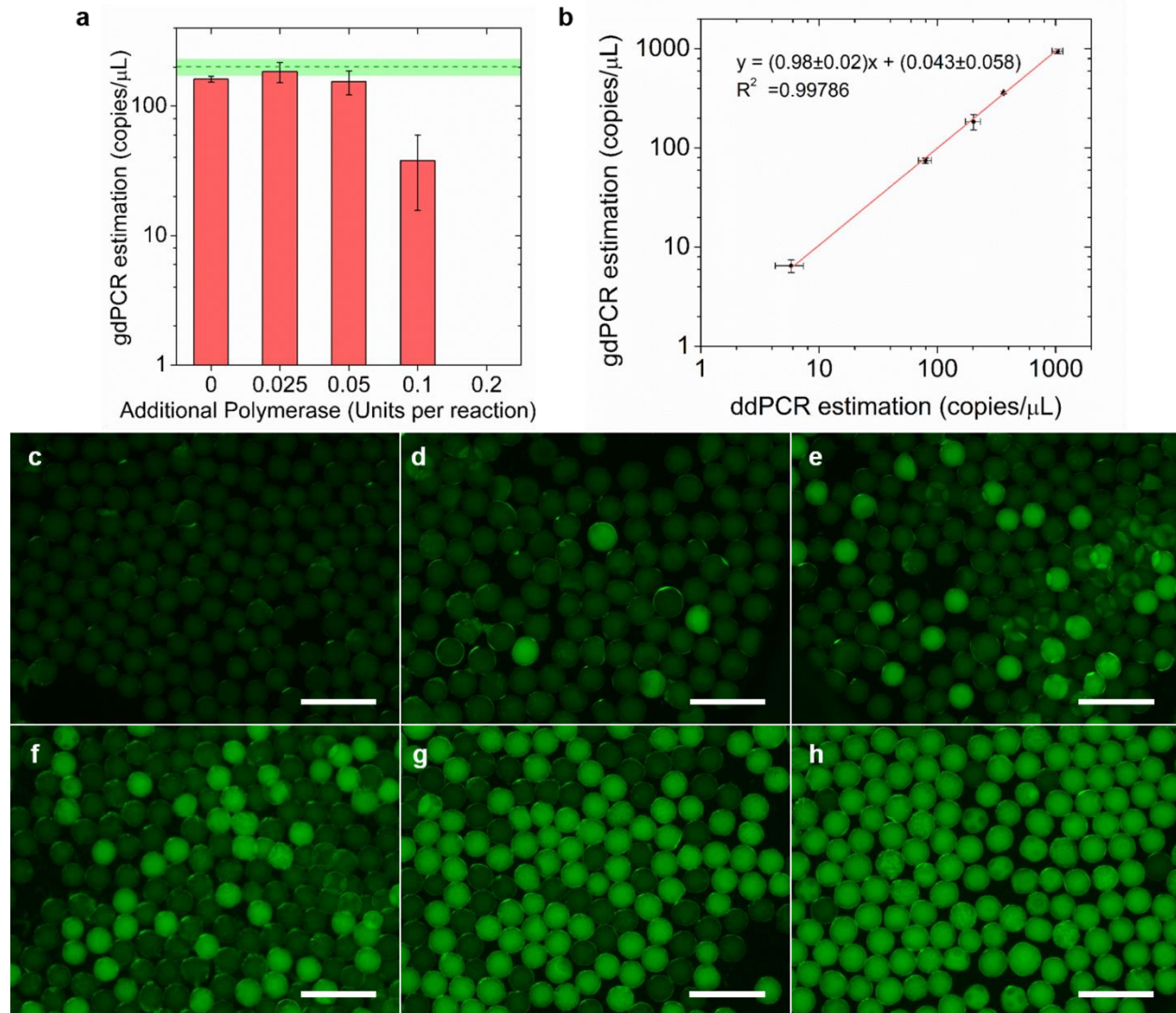
513 **Figure 1. Schematic of this study.** A hydrogel bead (Gelbeads)-based cell analysis platform was
514 developed for (a) digital molecular detection including PCR and LAMP and (b) single-cell
515 phenotypic analysis. The compartmentalization was realized by (c) a disposable centrifugal droplet
516 generation device. The dashed-line arrow indicates that the crosslinked hydrogel network grants
517 the potential of linking cell phenotype with *in situ* DNA/RNA characterization at single-cell
518 resolution.



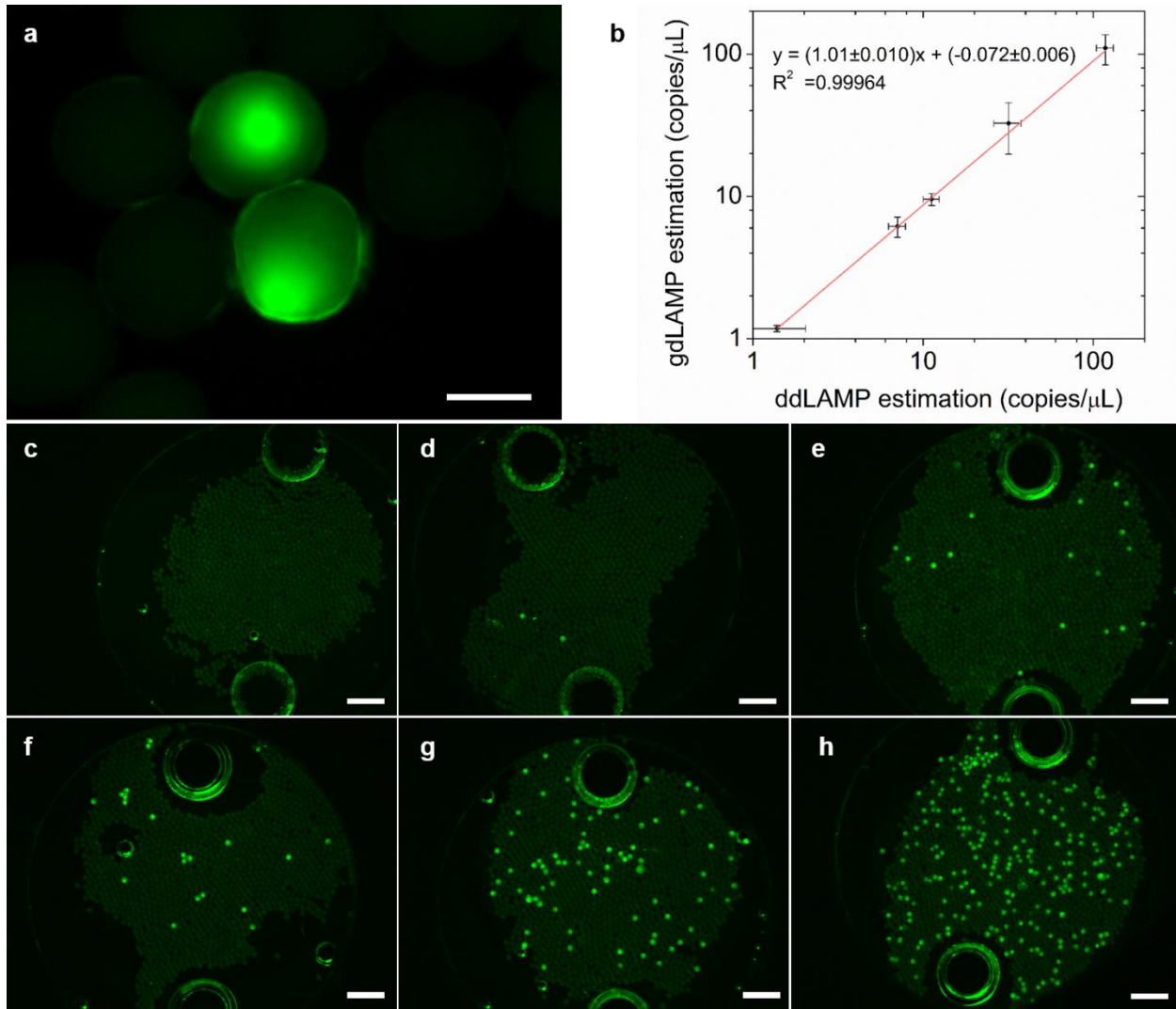
519 **Figure 2. Development and evaluation of disposable microfluidics for centrifugal droplet**
520 **generation.** (a) The device setup consisting of a 1.5-mL microcentrifuge tube holding the oil phase
521 and a needle with bent tip holding the aqueous reaction mixture in the Luer-lock. (b) A
522 representative fluorescence microscope image of generated droplets extracted into a viewing
523 chamber. The two large bright circles are ports on the viewing chamber for liquid loading Scale
524 bar, 1 mm. (c-f) Mean droplet size (black circles) and CV (blue circles) of droplets produced under
525 varying parameters including (c) oil phase volume, (d) needle inner diameter, (e) centrifugal
526 acceleration and (f) oil volume added to the Luer-lock. Error bars represent standard deviation
527 from independent triplicates.



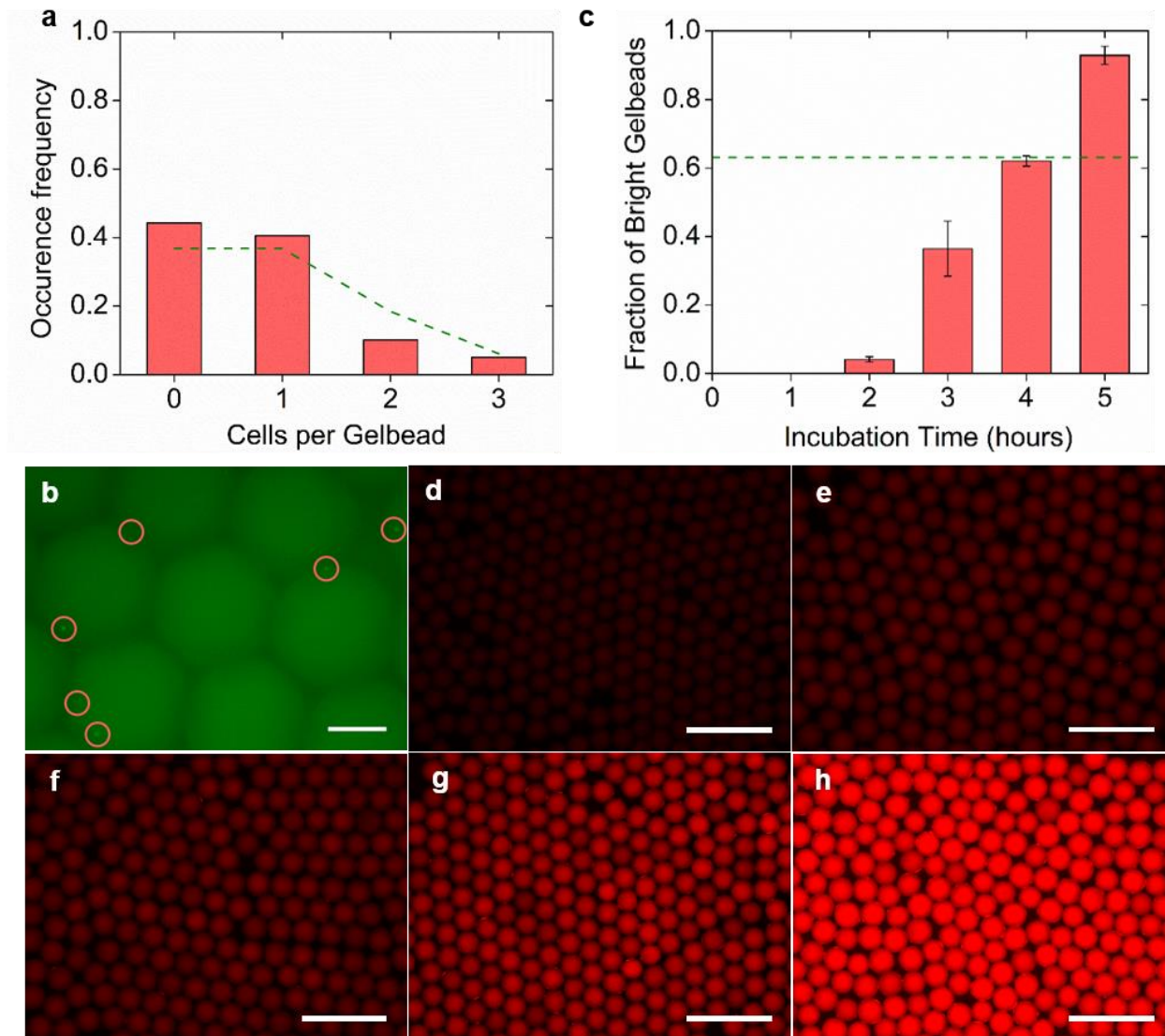
528 **Figure 3. Size characterization of droplets and Gelbeads.** The size distribution of droplets and
529 Gelbeads (a) generated in reaction matrices including PCR mix, LAMP mix, and culture media
530 mix, and (b) before and after heating program designated for PCR and LAMP. The line inside
531 each box represents the mean diameter; the lower and upper edges of each box respectively
532 represent 25% and 75% percentiles; the vertical bars below and above each box respectively
533 indicate 90th and 10th percentiles. The lower and upper red dots stand for outliers.



534 **Figure 4. Optimization and performance of gdPCR.** (a) The concentration estimations of
535 gdPCR assays for a fixed input *S. Typhi* DNA concentration (200 copies/μL) with varying
536 concentrations of additional polymerase. The green dashed line and the green area represent mean
537 concentration estimation with standard deviation of ddPCR assays from independent triplicates.
538 (b) With the optimized additional polymerase concentration (0.025 Units per reaction), the
539 correlation between gdPCR and ddPCR estimation for serial diluted target templates. Error bars
540 represent standard deviations from independent triplicates. (c-h) Example gdPCR fluorescent
541 images for no DNA input, and with 24000, 1500, 600, 300, 100 times dilution of harvested *S.*
542 *Typhi* DNA. Scale bars, 500 μm.



543 **Figure 5. Performance of gdLAMP.** (a) Connection of two positive Gelbeads after the gdLAMP
544 assay. Scale bar, 100 μ m. (b) The correlation between concentration estimations of gdLAMP and
545 ddLAMP assays for serial diluted target templates. Error bars represent standard deviation from
546 independent triplicates. (c-h) Example gdLAMP fluorescent images for no DNA input, and with
547 200, 100, 50, 20, 5 times dilution of harvested *S. Typhi* DNA. The two large bright circles on each
548 image are ports on the viewing chamber for liquid loading. Scale bars, 500 μ m.



549 **Figure 6. Single cell encapsulation validation and Single cell phenotyping performance in**
550 **Gelbeads.** (a) Number of cells encapsulated in each Gelbead counted and represented by
551 occurrence frequency. The dashed line represent theoretical values based on Poisson distribution.
552 (b) Example fluorescence image of encapsulated *S. Typhimurium* GFP cells (circled) for counting.
553 Scale bar, 100 μm . (c) The observed fraction of bright Gelbeads with varying incubation time,
554 with the dashed line representing 63% as Poisson distribution predicted based on the input cell
555 concentration. Error bars represent standard deviation from independent triplicates. (d-h) Example
556 images of Gelbeads containing *S. typhi* at the same input concentration incubated for 0, 2, 3, 4, 5
557 hrs. Scale bars, 500 μm .